Rapid production of protein-loaded biodegradable microparticles using surface acoustic waves

Mar Alvarez,[1] Leslie Y. Yeo,[1] James R. Friend,[1,a)] and Milan Jamriska[2]
[1]*Micro/Nanophysics Research Laboratory, Monash University, Clayton VIC 3800, Australia*
[2]*Defence Science & Technology Organisation, Human Protection & Performance Division (Aerosols), Melbourne, VIC 3001 Australia*

(Received 25 September 2008; accepted 24 November 2008; published online 21 January 2009)

We present a straightforward and rapid surface acoustic wave (SAW) atomization-based technique for encapsulating proteins into 10 μm order particles composed of a biodegradable polymeric excipient, using bovine serum albumin (BSA) as an exemplar. Scans obtained from confocal microscopy provide qualitative proof of encapsulation and show the fluorescent conjugated protein to be distributed in a relatively uniform manner within the polymer shell. An ELISA assay of the collected particles demonstrates that the BSA survives the atomization, particle formation, and collection process with a yield of approximately 55%. The SAW atomization universally gave particles with a textured morphology, and increasing the frequency and polymer concentration generally gave smaller particles (to 3 μm average) with reduced porosity. © *2009 American Institute of Physics.*
[DOI: 10.1063/1.3055282]

I. INTRODUCTION

The use of biodegradable polymeric microparticles as a vehicle to deliver proteins, peptides, and other therapeutic molecules for noninvasive administration offers a promising alternative to the current oral and injection routes. Encapsulation within the biodegradable polymeric excipient shields the drug from rapid hydrolysis and degradation, allowing its controlled release over time, thus prolonging the effect of the drug over longer periods of time while preventing dangerous dosage spikes. Encapsulation is a delicate procedure that can, however, damage the protein during the process through denaturization or aggregation.

It is therefore expedient to simplify the process as much as possible through the reduction of the processing time and steps required, and, in general, avoiding high *p*H and high temperatures during operation. Some of the most commonly employed methods to encapsulate proteins into polymer particles,[1] such as double solvent emulsion evaporation,[2] spray drying,[3] or phase separation,[4,5] present many disadvantages due to the use of high temperatures that can damage some temperature sensitive proteins or due to the presence of residual solvent.[6] These methods are also time consuming or inefficient due to the large number of steps required. Other techniques, such as electrohydrodynamic atomization, have also been employed for micro/nanoencapsulation of proteins using both dc (Refs. 7 and 8) and ac fields.[9,10] Although the possibility is reduced with the use of high frequency electric fields, the high voltages employed, typically 5–20 kV, could still pose potential risks in damaging the protein. Forde *et al.*[11] recently demonstrated the possibility for synthesizing 10 μm diameter protein-loaded polycaprolactone polymer particles using an ultrasonic atomizer. Nevertheless, the low frequencies (kHz order)[11–13] typically associated with ultrasonic atomization could still be insufficient to prevent denaturing of the protein due to the large shear rates involved during the atomization process.

a)Author to whom correspondence should be addressed. Electronic mail: james.friend@eng.monash.edu.au.

In this work we present preliminary results to show the feasibility of high frequency (MHz order) ultrasonic atomizers, specifically surface acoustic wave (SAW) atomizers, for the straightforward, rapid, and energy efficient production of protein-loaded polymer microparticles. A SAW is an electroacoustic wave, in this case a Rayleigh wave a few nanometers in amplitude, propagating on the surface of a piezoelectric substrate.[14] Unlike ultrasound, in which the acoustic energy is transmitted across the entire bulk of the material, the SAW energy is localized along the surface within a depth of three to four wavelengths into the substrate. As such, the transmission of energy into the fluid to be atomized is extremely efficient, with significantly less energy lost within the material itself. Roughly 33% of the acoustic energy passing beneath water placed on a SAW device is transmitted directly into the fluid.

SAW devices are already widely employed in a host of telecommunications applications, for example, as inexpensive multiplexing signal filters in mobile phones, demonstrating how they may be mass produced through standard microfabrication technology, and demonstrating the potential of these devices in the development of a miniaturized integrated device for *in situ* protein encapsulation for portable drug delivery. Alternatively, with scale-out techniques becoming an extremely attractive alternative to scale-up for high quality large-scale manufacture, we envisage the possibility of massively parallel arrays of these devices for mass production of protein-loaded microparticles. The benefits of scale-out are tremendous. A device can be taken offline for maintenance or replacement unlike a component in a manufacturing plant that would require complete plant shutdown.

In this work we provide a preliminary study using a model polymer/protein solution to show the feasibility of using SAW atomization as a rapid and simple means for encapsulating proteins within 10 μm order polymer microparticles. Besides elucidating the physical mechanism by which the particles are generated, we also examine the effect of the SAW device's working frequency and polymer concentration on the particle size and morphology.

II. MATERIALS AND METHODS

A. Polymer and protein solutions

Poly-ε-caprolactone [(PCL), MW ~65000, Sigma-Alrich, Australia], bovine serum albumin [(BSA), MW ~66 kDa, Sigma-Aldrich, Australia] and bovine albumin fluorescein isothiocyanate conjugate [(FITC-albumin), MW ~66 kDa, Sigma-Alrich, Australia] are employed in the study. Two different concentrations of PCL solution [0.2% weight/volume (w/v) and 1% w/v] were first prepared by dissolving PCL pellets in acetone through vigorous agitation at 40 °C. A 20 μl protein stock solution comprising either 10 mg/ml FITC-albumin or BSA in 10 mM Tris buffer (*p*H 7.0) is then added to 1 ml of the PCL solution. The polymer/protein solution is then dispensed onto the SAW device surface with the use of a syringe pump (KD Scientific, USA) at flow rates of 1.5 ml/h connected to a hypodermic syringe needle placed slightly above but not in contact with the substrate to maintain a constant drop size, 1 μl, on the SAW substrate.

For demonstrating safe atomization and encapsulation of the BSA protein, a BSA ELISA kit (Shibayagi Co. Ltd., Japan) was used to assess the concentration of BSA in the postatomized particles. The activity of the protein binding sites was tested through a "sandwich"-type immune assay, using plates initially coated with anti-BSA antibody. BSA protein released from the particles is then immobilized on the plate; after washing, peroxidase-conjugated antialbumin antibody (HRP–anti-BSA) was bonded. After another washing, a chromogenic substrate reagent (TMB) was added, developing color with intensities proportional to the concentration of bonded BSA. These color intensities directly indicate the concentration of natural BSA in the solution deposited in the assay. The protein was released from the atomized particles by dissolving the PCL excipient in chloroform and then adding phosphate buffered scaling (PBS) 1× for recovering the protein under physiological conditions (PBS 1×, *p*H 7, 37 °C). To accommodate the range of sensitivity of the chosen ELISA assay (<50 ng/ml), the samples were diluted 1:200 with PBS.

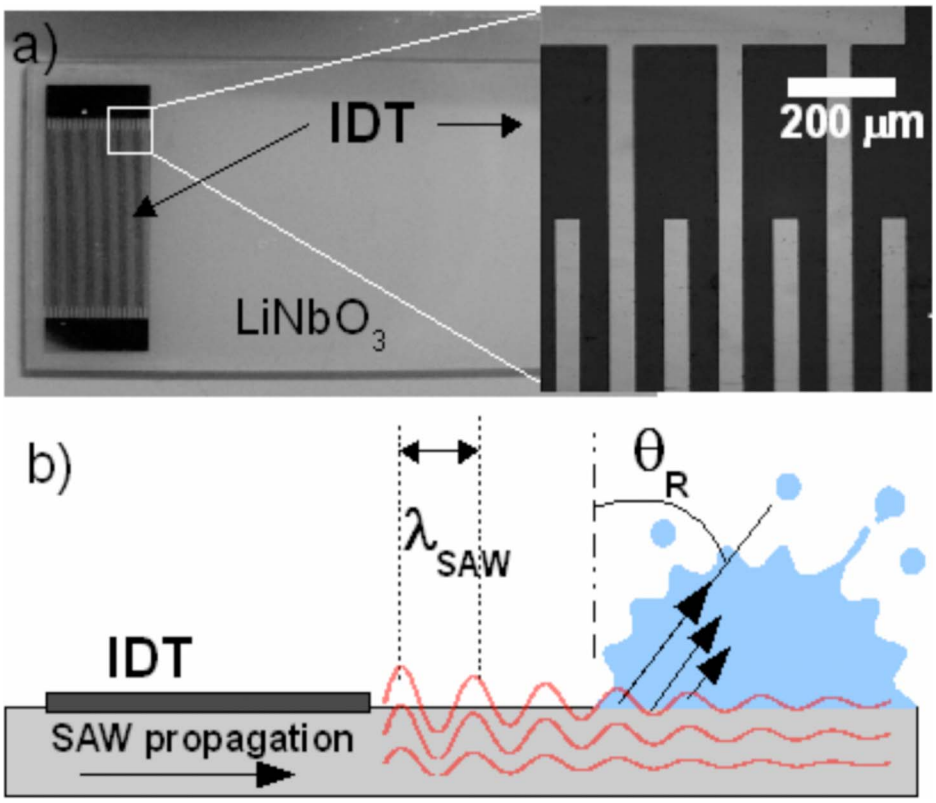

FIG. 1. (a) SAW device consisting of a single crystal lithium niobate piezoelectric substrate on which the interdigital transducer (IDT) electrode is patterned. A section of the IDT is enlarged to show the constituent finger pairs. (b) Schematic illustration (lateral view) of the surface acoustic wave propagation along the substrate and its interaction with a sessile liquid droplet. As a consequence of the diffraction of a significant amount of acoustic radiation into the drop at the Rayleigh angle θ_R, the drop interface is vigorously destabilized, resulting in its atomization into fine droplets that are ejected from the interface.

B. SAW devices

The SAW devices used in this work consist of a double port interdigital transducer (IDT) with 25 pairs of 400 nm thick, straight aluminum electrodes sputter-deposited onto a single crystal 127.68° *yx*-cut lithium niobate [($LiNbO_3$), Roditi, London, UK] piezoelectric substrate, as shown in Fig. 1(a). The IDT fabrication atop the piezoelectric substrate was performed using standard UV photolithography. The wavelength, λ_{SAW}, of the SAW is fixed by the width of both the IDT electrode fingers and the gaps between them. For the chosen substrate, the wave propagation speed, c_s, is approximately 3965 m/s, and hence the frequency is given by $f=c_s/\lambda_{SAW}$. SAW wavelengths of either 200 or 400 μm were employed, thus specifying the device operating frequency at 20 or 10 MHz, respectively. In order to generate the SAW, a sinusoidal electrical signal matching the operating frequency is applied to the IDT using a RF signal generator (N9310A, Agilent, USA) and RF power amplifier (10W1000C, Faraday Pty. Ltd., Australia).

C. Particle synthesis and characterization

Protein-loaded polymer microparticles are produced by postatomization evaporation of the solvent, i.e., acetone, as the ejected droplets travel in-flight through a heated drying tube before they impact a collection surface or solution of deionized (DI) water with a small amount of surfactant, either 1 mM sodium dodecyl sulphate (Sigma-Aldrich, Australia) or 0.1% v/v Tween-20 (Sigma-Aldrich, Australia). The choice of surfactant or its concentration is not expected to significantly alter the particle size,[15] but does help prevent agglomeration at the fluid collection

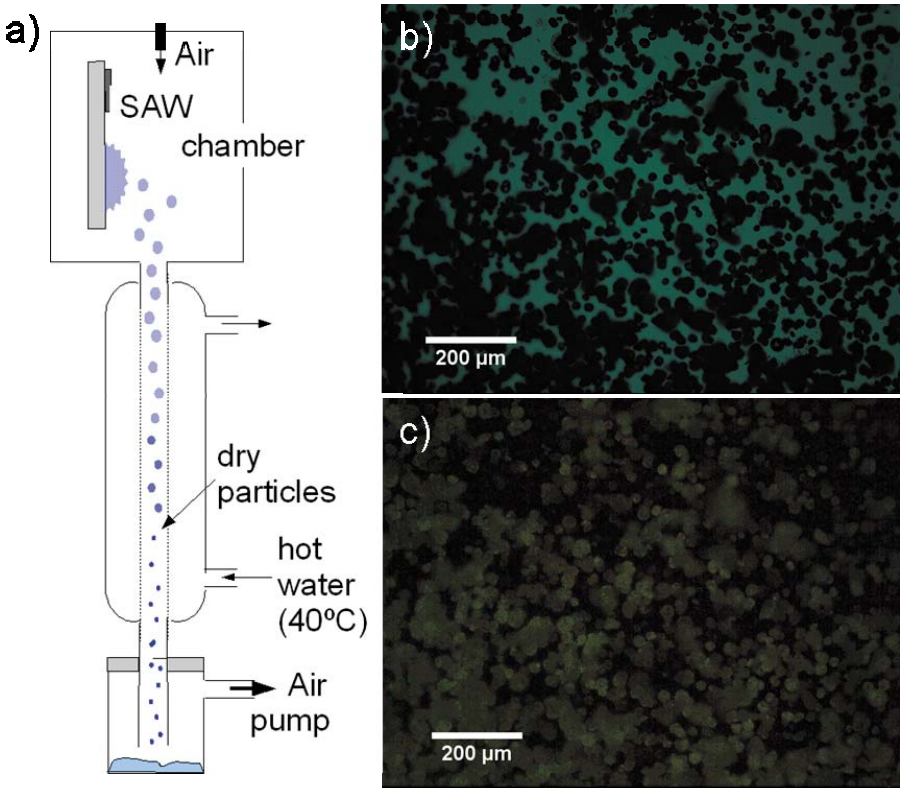

FIG. 2. (a) Schematic diagram of the experimental setup used for drying and collecting the particles. (b) Representative image of the protein-loaded polymeric particles collected over a glass substrate, taken with an optical microscope. (c) Same image in (b) obtained through fluorescence microscopy.

surface. A schematic of the experimental setup used is shown in Fig. 2(a), where the particle trajectories are aided through an airflow generated by a vacuum pump placed distally to the entire setup. To ensure sufficient drying of the polymeric excipient so that they do not shatter or splatter upon impact onto the collection medium, a trajectory length of 50 cm is maintained. Figures 2(b) shows examples of the polymeric particles collected over 30 s on a glass substrate held at the bottom of the drying tube where the particles exit, as obtained through bright-field microscopy (BXFM, Olympus, Japan). Due to the particle density, the same image is viewed under fluorescence microscopy (BXFM, Olympus, Japan) to aid visualization [Fig. 2(c)] using the fluorescent signal emitted by the FITC-albumin.

Scanning electron microscopy [(SEM), S570, Hitachi, Japan] was employed to inspect the size and morphology of the particles. As above, the particles were collected over a plate placed at the bottom of the drying chamber. The samples were scanned with SEM at 15 kV after being vacuum coated with a thin layer of gold. The SEM images were analyzed using imaging processing software (ImageJ, National Institutes of Health, USA) to obtaining the particle size distribution.

Particle samples loaded with FITC-albumin were also observed through confocal laser scanning microscopy (FluoView FV1000, Olympus, Japan) as proof of encapsulation. In this case, the plate containing the particles was first rinsed using DI water to remove traces of the protein external to the particles with the aid of a porous membrane microfilter (Type-GS 0.22 μm, Millipore, USA). The plate was then mounted over a glass slide using a mounting agent to fix the particles, taking extreme care not to deform them, and scanned at an excitation wavelength of 495 nm with a 40× oil lens.

III. RESULTS AND DISCUSSION

A. Ejection mechanism, particle size, and surface morphology

We describe here briefly the mechanisms by which the polymer microparticles are generated.[15,16] Due to the difference in the sound velocity in the liquid ($c_w \approx 1485$ m/s for water) and in the solid substrate ($c_s \approx 3965$ m/s), the SAW leaks into the drop at an angle known as the *Rayleigh angle*, $\theta_R = \sin^{-1}(c_w/c_s) \approx 22°$ to the vertical axis, as illustrated in Fig. 1(b). This consequently produces a compressional wave within the liquid drop that drives fluid recirculation known as *acoustic streaming*.[17] Besides producing a strong body force on the drop, which can be harnessed for rapid drop transport in microfluidic systems,[18] the acoustic streaming can also be exploited for a variety of microfluidic manipulations such as microchannel pumping,[19] micromixing,[20] microparticle concentration/separation[20,21] and sorting,[22] and bioscaffold cell seeding,[23] among others. At high applied powers, however, another phenomenon is observed in which the violent destabilization of the drop interface takes place, giving rise to the pinch-off of droplets and jets off the interface.[24] It is this atomization process[15,16,24–26] that was used to synthesize solid PCL and protein nanoparticles,[15,16] as well as to pattern ordered arrays of polymer spots onto substrates,[27] and which we shall employ here for the protein encapsulation.

Due to the wave reflection at the edge of the device, the SAWs produced in this work are not pure traveling waves, but contain a standing wave component that further contributes to the amplification and destabilization of the capillary waves at the drop interface. To understand the dynamics involved, we image the atomization process using a high-speed digital video camera (MC1310, Mikroton, Germany) connected to a long distance microscope (K2, Infinity, USA) at 2000–3000 frames/s.

Typical stages of the atomization process are captured in Fig. 3. A drop of polymer solution dispensed onto the device substrate is observed to translate in the SAW propagation direction due to its traveling wave component, as observed in Fig. 3(a). The translation speeds are fast, typically 1–10 mm/s, which is one to two orders of magnitude faster than the speeds achieved through electrowetting-driven droplet transport, making SAWs an attractive alternative for this purpose.[27,28] As the drop translates, it leaves behind a trailing film that is approximately 10 μm thick. Nevertheless, due to the large amounts of acoustic energy that leak into both the film and the drop, capillary waves that appear on the free surface of the film or drop are rapidly and violently destabilized. Through laser Doppler vibrometry, we have shown in a previous study[24] that as long as the film or drop dimension is *larger* than the boundary layer thickness

$$\delta \sim \left(\frac{\mu}{\rho\omega}\right)^{1/2}, \tag{1}$$

viscous effects dominate over inertial effects; excitation with this arrangement gives capillary waves possessing oscillation frequencies of a rather broad range (around one order of magnitude) but centered around the *viscous-capillary resonant frequency*,[27]

$$f_c \sim \frac{\gamma}{\mu L}. \tag{2}$$

This is the case even though excitation at these frequencies generates large accelerations, on the order of 10^7 m/s^2, of the fluid's free surface. In the above, μ is the fluid viscosity, ρ its density, ω the SAW frequency, γ the surface tension, and L the characteristic film or drop dimension. Typically, $\delta \sim 10^{-6}$ m and hence the film would have to be extremely thin before the capillary waves on its interface are driven by capillary-inertia resonance. In the cases reported here, $f_c \sim 10–10^2$ kHz.

It can be seen that from Fig. 3(b) that the capillary waves destabilize to form an elongated jet, which eventually necks and pinches off to form a droplet. It is the wavelength of the capillary waves therefore that sets the ejected jet/droplet size,[24]

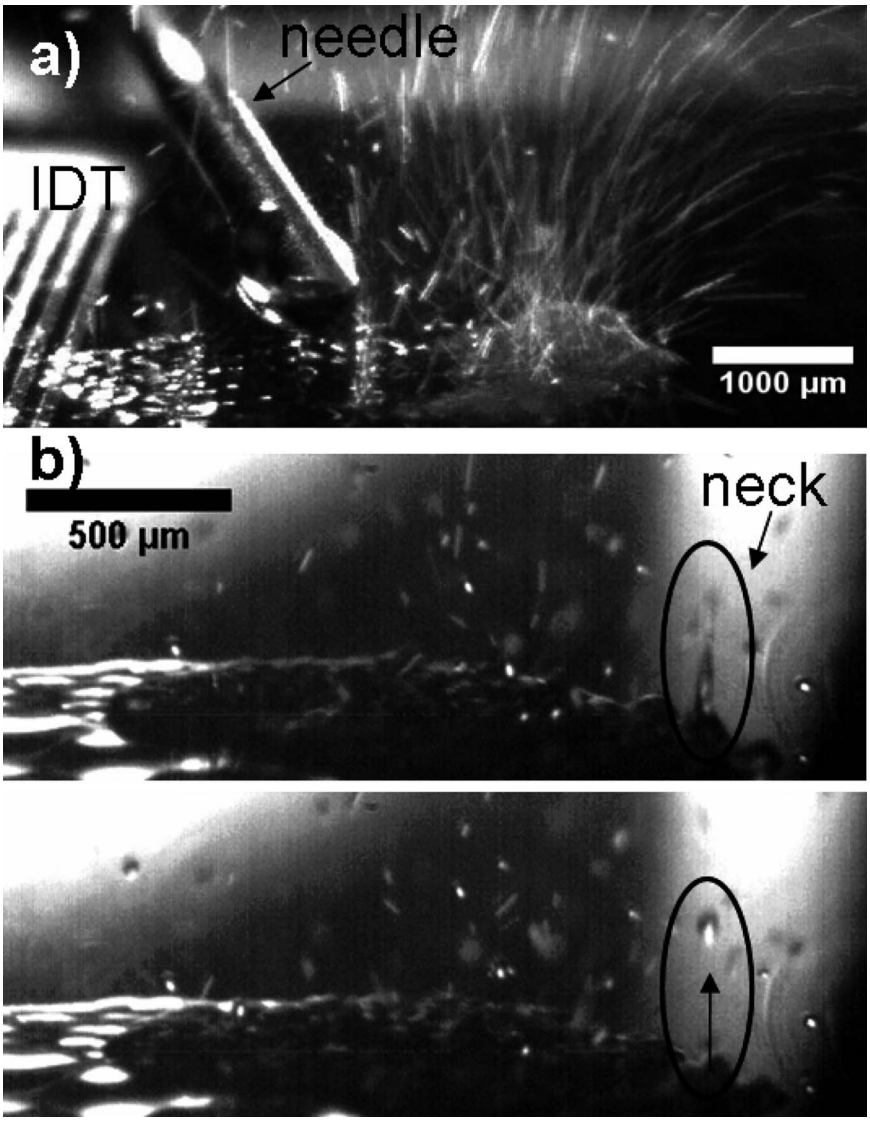

FIG. 3. Representative images of the atomization process acquired through high-speed visualization with a 10 MHz device. In (a), the drop containing the polymer solution is delivered via a syringe pump through the needle and deposited on the piezoelectric substrate. The drop then translates rapidly from left to right in the direction of the SAW propagation; note that the SAWs contain both traveling and standing wave components. As it translates, the drop leaves behind a thin film, which almost cannot be seen. Atomization occurs off the drop interface as well as the thin film. In the latter case, this is responsible for highly ordered regular polymer spot patterns on the substrate.[27] In this case, the polymer concentration is 0.2% w/v and the images were captured at 2000 frames/s. In (b), two successive images capture the process by which droplets are atomized off the interface of the thin trailing film. We note the destabilization of the capillary waves along the interface leads to the formation of a jet, which eventually necks and pinches-off to form the ejected droplet. Given that the images were captured at 3000 frames/s, the time interval between the two images are approximately 0.3 ms. In this case, the polymer concentration is 1% w/v.

$$\lambda \sim \left(\frac{2\pi\gamma}{\rho f_c^2}\right)^{1/3}. \tag{3}$$

Given the orders of magnitude for f_c above, we expect $\lambda \sim 10^{-4}-10^{-5}$ m. This is confirmed through the plan-view images of the trailing film—the capillary waves induced on the free surface of the film, be it a pure polymer film [Fig. 4(a)] or one containing BSA [Fig. 4(b)], is typically on the order 10^{-4} m. Similar dimensions are also typically observed for the jet diameter as well as the

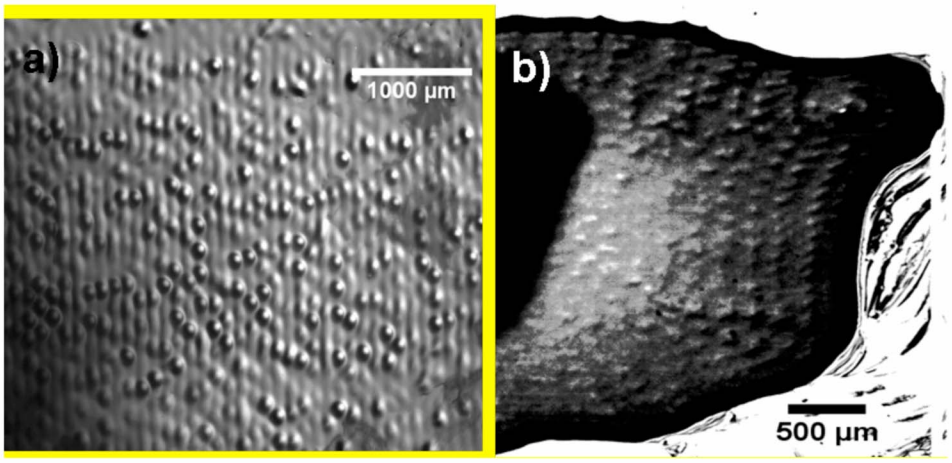

FIG. 4. Capillary waves formed on the surface of the trailing film comprising the (a) polymer solution ($\lambda \approx 100$ μm), and, (b) polymer/BSA solution ($\lambda \approx 200$ μm), as viewed directly from above. A 20 MHz SAW device is used in this case and the images were acquired through a camera connected to a microscope.

ejected droplet diameter. We note that the larger 10^{-4} m droplets have a tendency to drop back to the surface due to their relatively large masses and so the droplet (and hence particles, as we shall discuss below) sizes obtained are on the order of 10 μm. Moreover, the 0.1 ms order time [the time between the two successive frames in Fig. 3(b)] for the jet to break up due to long-wave axisymmetric instabilities leading towards viscous film drainage and rupture is roughly consistent with the viscous-capillary pinch-off time governed by Eq. (2).

Evaporation of the solvent in flight as the atomized droplets are transported through the heated tube illustrated in Fig. 2(a) then leaves behind a hardened polymer shell. Given that the strong acoustic streaming drives effective mixing within the pre-atomized drop,[20] the polymer/protein solution is well mixed prior to atomization, and hence it is conceivable that the protein is atomized together with the polymer solution and encapsulated within the polymer shell, although we shall seek to prove this conjecture subsequently in the next subsection.

The protein-loaded particle sizes are summarized in Table I as a function of several different device/polymer solution concentration combinations. We observe the particle size to decrease with increasing SAW frequency, as predicted by Eq. (3), although there is insufficient frequency data to quantitatively show the $\lambda \sim f^{-2/3}$ scaling; the matching is rather poor. Nevertheless, the 10 μm order dimension of the particles correspond to the predictions of the scaling theory in Eq. (3).

Figures 5 and 6 show the effect of the polymer concentration and SAW frequency on the particle morphology. These SEM images in Fig. 5(a) reveal hollow particles with high porosity for the lower polymer concentration (0.2% w/v) and lower working frequency (10 MHz). As the polymer concentration and the working frequency are increased, the particles appear to become

TABLE I. Mean particle diameter for different combinations of the SAW frequency and polymer concentrations employed.

Sample	Frquency (MHz)	PCL concentration (% w/v)	BSA solution (ml)	Mean particle diameter ±std dev (μm)
A	10	0.2	20	23.0 ± 5.9
B	10	1	20	14.6 ± 6.3
C	20	0.2	20	6.7 ± 2.6
D	20	1	20	7.3 ± 3.0

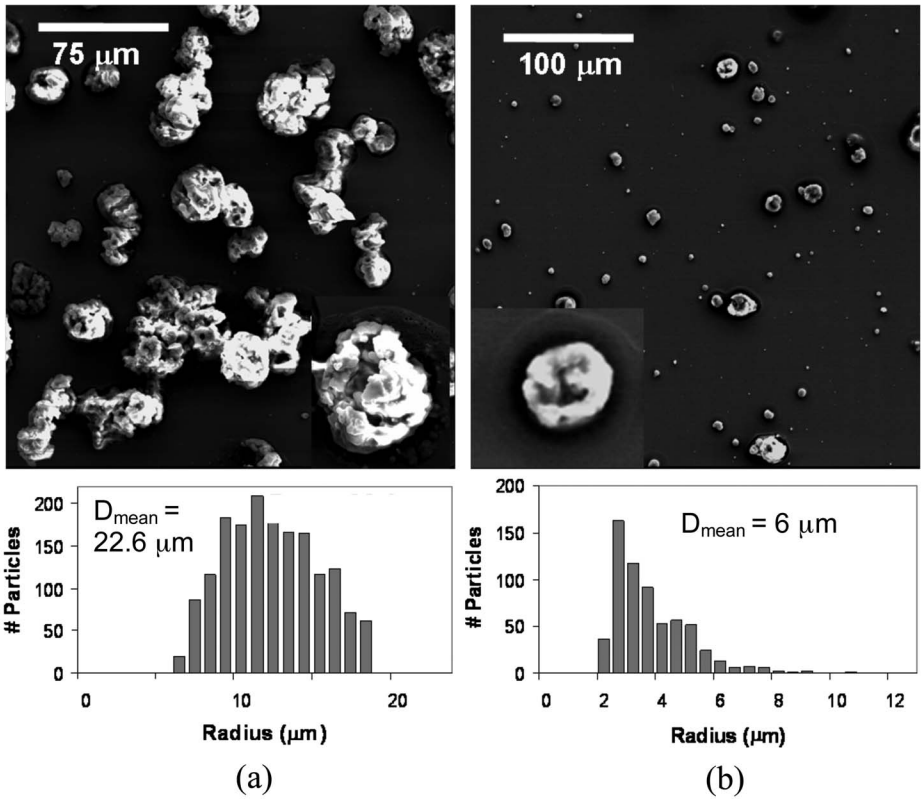

FIG. 5. SEM images of a representative sample of BSA-loaded polymer particles and produced with (a) 10 MHz (sample A) and (b) 20 MHz SAW (sample C) devices, for an initial polymer concentration of 0.2% w/v, and their corresponding size distributions.

less porous and slightly more homogeneous [Figs. 5(b) and 6(b)]. In all of the particles, however, the surfaces appear to have a microtextured surface that resembles grape bunches.

The particle morphology is attributed to the poor dissolution of PCL in acetone due to the close matching between the solubility parameters, promoting fast evaporation and phase separation of the solvent.[15,29,30] The rapid evaporation of the solvent results in a solidified polymer film being formed, thus encapsulating the remaining solution within. However, rapid quenching of the temperature during the solvent evaporation process also triggers a thermodynamic instability that induces phase separation to occur through spinodal decomposition, creating polymer-rich and solvent-rich zones in the surrounding polymer film.[15,31] As a consequence of these spatial nonuniformities in the concentration, a large number of nucleation sites are formed which results in the clustering of PCL molecules that constitute the grapelike surface microstructured texturing observed in all of the particles in Figs. 5 and 6 in a manner akin to evaporation-driven template-induced crystalline self-assembly in colloidal systems.[15,32]

On the other hand, the solvent shut inside the droplet could also be expulsed through the film, resulting in the collapse of the shell and the formation of hollow porous particles in Figs. 5(a) and 6(a). The formation of solid spheres rather than collapsed particles depends on the vapor pressure and the initial droplet size.[33] The shell formation and subsequent collapse is typically found in relatively large droplets[34] consistent with the higher porosity found for the larger ($\sim$20 μm) particles generated with the 10 MHz device (Table I).

The particle size and morphology is not affected by the protein loading for this particular choice of excipient, protein, and atomization settings. Close examination of the SEM images of unloaded polymer particles produced with the 20 MHz device and 1% w/v PCL in Fig. 7 shows a similar size (7.67 ± 3.0 μm) and morphology to the protein-loaded particles (7.3 ± 3.0 μm) in Fig.

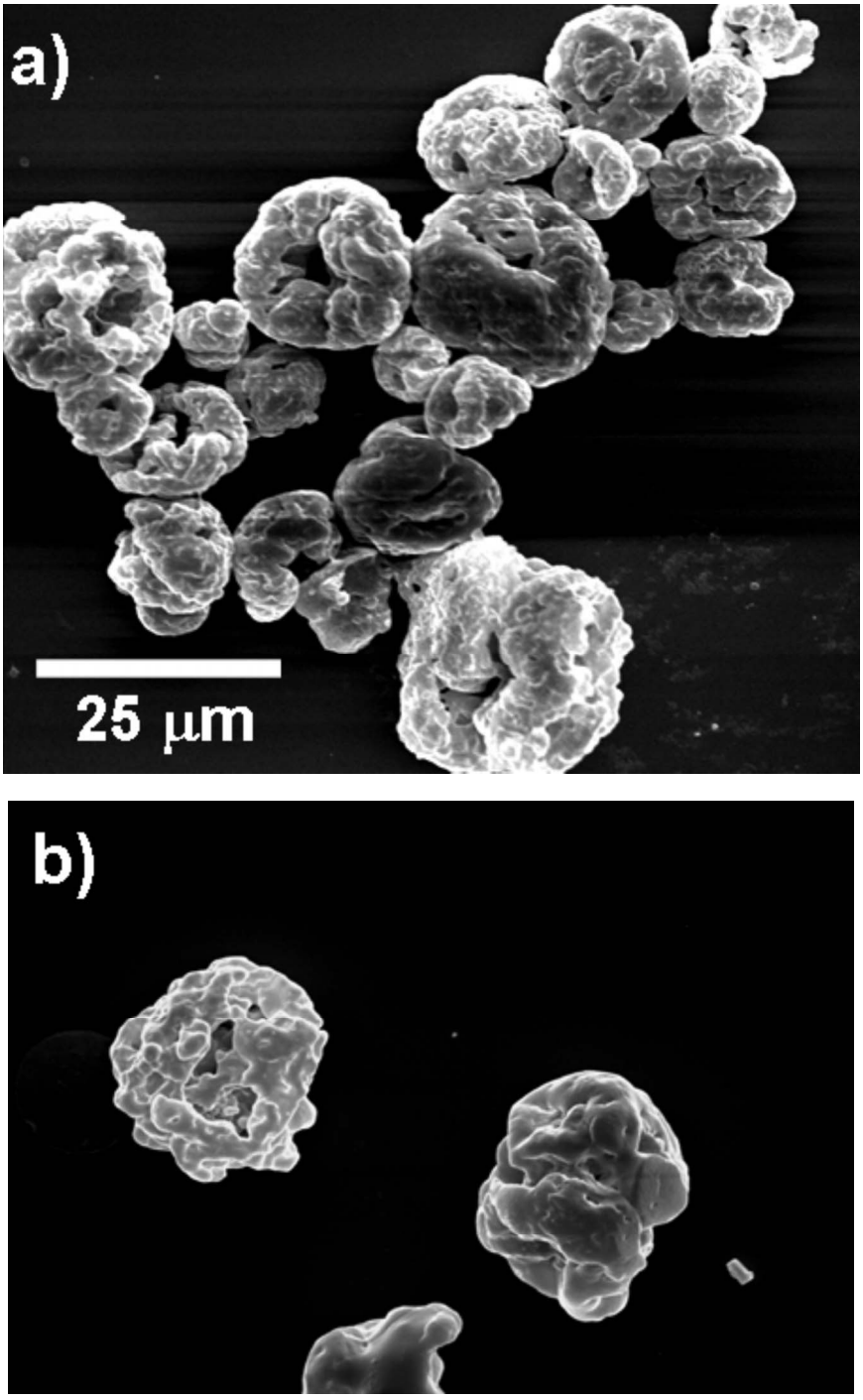

FIG. 6. SEM images of representative samples of BSA-loaded polymer particles produced with (a) 10 MHz (sample B) and (b) 20 MHz (sample D) SAW devices for an initial polymer concentration of 1% w/v.

6(b). It is therefore likely that the particle size and morphology is mainly controlled by the polymer concentration and evaporation of the solvent evaporation, consistent with other studies.[33]

Smaller particles with smoother surface morphologies can be generated by reducing the vacuum suction rate and inverting the drying configuration in Fig. 2(a) to face upwards. Figure 8 shows a comparison between the 7 μm diameter particles with textured surfaces obtained previ-

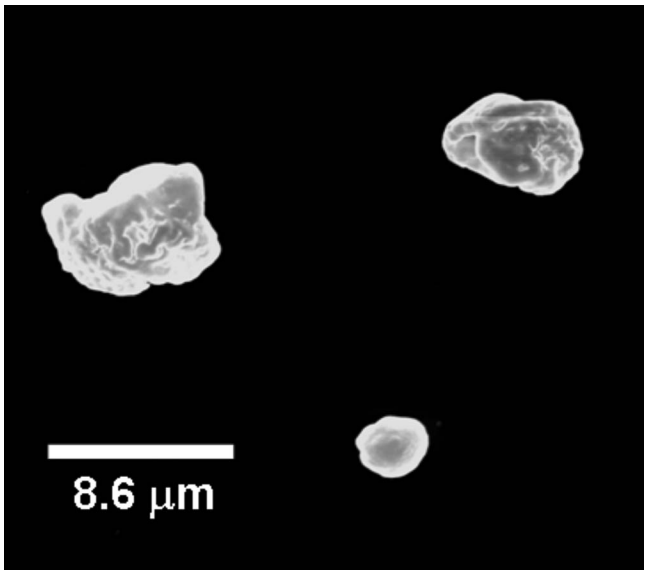

FIG. 7. SEM image of a representative sample of unloaded PCL polymer particles produced with a 20 MHz SAW device for an initial polymer concentration of 1% w/v.

ously [Fig. 8(a)] with the smooth 3 μm diameter particles obtained with the decreased air flow and inverted setup [Fig. 8(b)]. The decreased droplet speed through the drying tube and the reduced solvent evaporation rate allows more uniform evaporation throughout the entire droplet, thus reducing the probability of nucleation and poration. The choice of working conditions and solvent therefore plays an important role in the final particle size and morphology.

B. Proof of protein encapsulation

As proof that the protein is encapsulated within the polymer shell instead of being superficially bonded to the shell exterior, we examined the fluorescent signals emitted by the FITC-

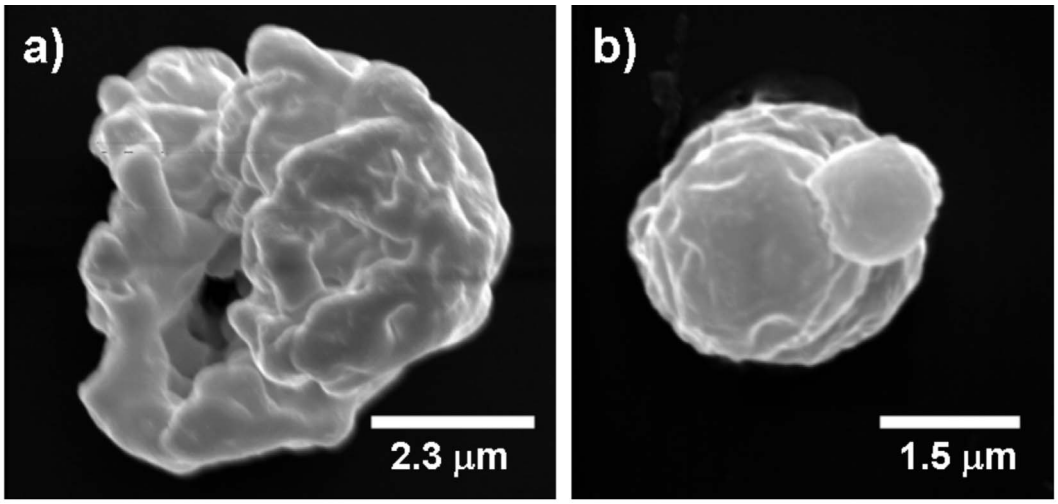

FIG. 8. SEM images of two protein-loaded PCL polymer particles produced with a 20 MHz SAW device with an initial polymer concentration of 1% w/v. Image (a) shows a representative particle obtained through the drying tube configuration in Fig. 2(a), whereas image (b) shows a representative particle obtained through inverting the drying tube configuration and reducing the air flow rate.

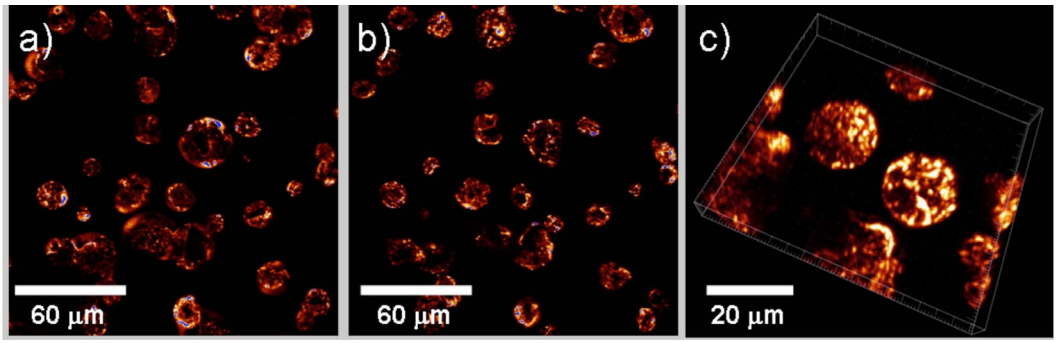

FIG. 9. Planar confocal laser scanning microscopy images taken at vertical positions (a) near the bottom and (b) close to the center of the particles showing the distribution of the fluorescent conjugated BSA within the PCL shell. Image (c) is a three-dimensional reconstruction of a number of these two-dimensional planar scans.

albumin through confocal laser scanning microscopy after rinsing the particles through DI water to remove external traces of the protein. Two-dimensional planar scans were conducted at various confocal slices through the particles to examine the protein distribution inside the particles. The maximum distance traversed along the vertical z axis was approximately 20 μm, matching the particle sizes obtained with SEM for this device and polymer concentration (sample B). Although several images were acquired at various vertical depths, Figs. 9(a) and 9(b) show scans at vertical positions corresponding to the bottom of the particle close to the substrate and at the center of the particle, respectively, which are representative of scans observed at other positions. A qualitative inspection, at least, shows comparable fluorescent signal intensities in both cases. A three-dimensional reconstruction of the confocal images is shown in Fig. 9(c), effectively showing the protein distribution within the entire particle. While these figures do not permit adequate quantification, they at least provide preliminary qualitative evidence that the proteins are encapsulated within the polymer shells, and that the distribution within is fairly uniform.

C. Protein function

Preliminary results obtained using ELISA demonstrated that 54% of the BSA protein survived atomization, was collected in the sampling solution, and successfully emerged from the particles with its functional groups intact. The ELISA was run twice with color assessments performed in triplicate; 54 μg of BSA was indicated in the original, undiluted sample by the test with standard deviation of 6.7, obtained from 100 μg of BSA in 500 μl of stock polymer/protein solution that was atomized by the device.

IV. CONCLUSIONS

We demonstrate the possibility of simple and rapid encapsulation of proteins within 10 μm order biodegradable polymer particles through a SAW atomization process, using BSA as a representative protein, with 54% efficiency in delivery with a crudely controlled prototype. Confocal microscopy slices through the particles show, at least qualitatively, that the fluorescent conjugated bovine serum albumin are encapsulated and uniformly distributed within. In addition, we investigated the physical mechanism by which the particles are generated and examined the dependence of the particle size and morphology on various parameters, such as the SAW working frequency and polymer concentration. The lower frequency produced larger particles with 20 μm mean diameter. These larger particles are observed to be more susceptible to poration as a result from the expulsion of residual solvent trapped within the hardened polymer shell, and hence possess morphologies that are hollow and porous. With higher frequencies, smaller particles under 10 μm were produced with a reduction in both porosity and hollow morphology. In both cases, however, the particle surfaces were found to be textured with microstructures arising due to nucleation templating as a consequence of inhomogeneous solvent concentration produced by the rapid

evaporation process. By reducing the evaporation rate, smaller and smoother particles can be generated. The reduction of the particle size to 3 μm at least shows that particles suitable for effective pulmonary drug delivery (particles between 1 μm and 5 μm are required for optimum dose delivery) can be produced through this method. These results therefore demonstrate the feasibility of SAW atomizers for the encapsulation of drugs in biodegradable polymer microparticles for controlled noninvasive drug delivery. The relatively low powers employed, typically between 1–5 W, present significant advantages over conventional low frequency atomizers where 50–100 W of power are usually required.

ACKNOWLEDGMENTS

We would like to thank the Australian Research Council and Nanotechnology Victoria for support of this work via Grants No. DP0666660, No. DP0773221, No. LE0668435, and No. DH004. Helpful advice and discussions with Dr. John Tzong-Hsien Lee, Department of Biochemistry and Molecular Biology, Monash University, is gratefully acknowledged.

[1] H. Tamber, P. Johansen, H. P. Merkle, and B. Gander, Adv. Drug Delivery Rev. **57**, 357 (2005).
[2] M.-A. Benoit, B. Baras, and J. Gillard, Int. J. Pharm. **184**, 73 (1999).
[3] B. Gander, P. Johansen, H. Nam-Tran, and H. P. Merkle, Int. J. Pharm. **129**, 51 (1996).
[4] V. Coccoli, A. Luciani, S. Orsi, V. Guarino, F. Causa, and P. A. Netti, J. Mater. Sci.: Mater. Med. **19**, 1703 (2008).
[5] T. Morita, Y. Sakamura, Y. Horikiri, T. Suzuki, and H. Yoshino, J. Controlled Release **69**, 435 (2000).
[6] C. Thomasin, P. Johanson, R. Alder, R. Bemsel, G. Hottinger, H. Altorfer, A. D. Wright, E. Wehrli, H. P. Merkle, and B. Gander, Eur. J. Pharm. Biopharm. **42**, 16 (1996).
[7] Y. Wu and R. L. Clark, J. Colloid Interface Sci. **310**, 529 (2007).
[8] I. G. Loscertales, A. Barrero, I. Guerrero, R. Cortijo, M. Marquez, and A. M. Gañán-Calvo, Science **295**, 1695 (2002).
[9] L. Y. Yeo, Z. Gagnon, and H.-C. Chang, Biomaterials **26**, 6122 (2005).
[10] L. Y. Yeo and H.-C. Chang, in WIT Trans. Eng. Sci. **52**, 223 (2006).
[11] G. M. Forde, A. D. Coomes, F. K. Giliam, Y. Han, and M. J. Horsfall, Trans. IChemE Part A **84**, 178 (2006).
[12] S. Freitas, H. P. Merkle, and B. Gander, J. Controlled Release **95**, 185 (2004).
[13] H. R. Costantino, L. Firouzabadian, K. Hogeland, C. Wu, C. Beganski, K. G. Carrasquillo, M. Córdova, K. Griebenow, S. E. Zale, and M. A. Tracy, Pharm. Res. **17**, 1374 (2000).
[14] R. M. White and F. W. Volmer, Appl. Phys. Lett. **7**, 314 (1965).
[15] J. R. Friend, L. Y. Yeo, D. R. Arifin, and A. Mechler, Nanotechnology **19**, 145301 (2008).
[16] M. Alvarez, J. R. Friend, and L. Y. Yeo (unpublished).
[17] A. Wixforth, C. Strobl, C. Gauer, A. Toegl, J. Scriba, and Z. v Guttenberg, Anal. Bioanal. Chem. **379**, 982 (2004).
[18] L. Y. Yeo and J. Friend, Biomicrofluidics **3**, 012002 (2009).
[19] M. K. Tan, L. Y. Yeo, and J. R. Friend (unpublished).
[20] R. Shilton, M. K. Tan, L. Y. Yeo, and J. R. Friend, J. Appl. Phys. **104**, 014910 (2008).
[21] H. Li, J. R. Friend, and L. Y. Yeo, Biomed. Microdevices **9**, 647 (2007).
[22] H. Li, J. R. Friend, and L. Y. Yeo, Phys. Rev. Lett. **101**, 084502 (2008).
[23] H. Li, J. R. Friend, and L. Y. Yeo, Biomaterials **28**, 4098 (2007).
[24] A. Qi, J. R. Friend, and L. Y. Yeo, Phys. Fluids **20**, 074103 (2008).
[25] M. Kurosawa, T. Watanabe, and T. Higuchi, in *Proceedings of the IEEE Conference on Micro Electro Mechanical Systems MEMS 1995*, Amsterdam, The Netherlands (IEEE, Pistacaway, NJ, 1995), pp. 25–30.
[26] K. Chono, N. Shimizu, Y. Matsui, J. Kondoh, and S. Shiokawa, Jpn. J. Appl. Phys., Part 1 **43**, 2987 (2004).
[27] M. Alvarez, J. R. Friend, and L. Y. Yeo, Langmuir **24**, 10629 (2008).
[28] L. Y. Yeo, D. Lastochkin, S.-C. Wang, and H.-C. Chang, Phys. Rev. Lett. **92**, 133902 (2004).
[29] J. C. Huang, K. T. Lin, and R. D. Deanin, J. Appl. Polym. Sci. **100**, 511 (2002).
[30] Z. G. Tang, R. A. Black, J. M. Curran, J. A. Hunt, N. P. Rhodes, and D. F. Williams, Biomaterials **25**, 4741 (2004).
[31] L. Y. Yeo and J. R. Friend, J. Exp. Nanosci. **1**, 177 (2006).
[32] J. P. Hoogenboom, C. Rétif, E. de Bres, M. van de Boer, A. K. van Langen-Suurling, J. Romijn, and A. van Blaaderen, Nano Lett. **4**, 205 (2004).
[33] J. Raula, H. Eerikainen, and E. Kauppinen, Int. J. Pharm. **284**, 13 (2004).
[34] K. H. Leong, J. Aerosol Sci. **18**, 511 (1987).